Nonlocal response of electric and magnetic modes in a silver cuboid dimer

Xianghao Zeng (曾翔昊), Yong Wang (王 勇), Yonghua Lu (鲁拥华), and Pei Wang (王 沛)*

Department of Optics and Optical Engineering, Anhui Key Laboratory of Optoelectronic Science and Technology, University of Science and Technology of China, Hefei 230026, China

**Corresponding author: wangpei@ustc.edu.cn*

Received March 16, 2016; accepted May 5, 2016; posted online June 13, 2016

The nonlocal effect on the spontaneous emission of a silver cuboid dimer is investigated using a local analog model. Magnetic as well as electric dipole excitations are introduced to excite different gap modes. The nonlocal response of electric and magnetic modes on various parameters of gap (width and refractive index) are investigated. Unidirectional radiation is achieved by the interaction between electric and magnetic modes in both local and nonlocal models. Compared to local simulations, the resonant wavelength is blue shifted and the spontaneous emission enhancement is weakened in the nonlocal model. The relative shifts of the resonant wavelengths get larger in smaller gaps with a higher refractive index.

OCIS codes: 250.5403, 260.2510.
doi: 10.3788/COL201614.072501.

An enhanced electromagnetic field in tiny gaps between metallic nanostructures has been widely applied to fields such as surface-enhanced Raman scattering[1–3], plasmonic sensing[4,5], nanolasing[6,7], and enhanced spontaneous emission[8,9]. The progress in nanofabrication technologies and chemical synthesis has pushed the critical dimension of gaps and nanoparticles to the order of nanometers and below[10–12]. In such circumstances, the classical local-response approximation (LRA) for free electron response inside metallic structures is insufficient to describe the light-matter interactions because the metal charges are not distributed exactly on the surface as assumed by the LRA. So, by considering the fact that the charge density spreads into the metal nanoparticles, a hydrodynamic model is introduced to analyze the nonlocal responses of noble metals[12–16]. It should be noted here that film-coupled metal nanocube structures or a metal cuboid dimer support both electric and magnetic resonances[17–20]. Previous nonlocal studies were mostly focused solely on electric responses[16], and magnetic modes are seldom investigated.

In this Letter, we numerically analyze the spontaneous emission enhancement of a silver cuboid dimer using a local analog model (LAM), which is proposed based on the nonlocal hydrodynamic model to simplify the numerical simulation of nonlocal responses of nanoparticles and metal-insulator-metal (MIM) structures[21]. We take the nonlocal effect on the magnetic response into consideration. It causes the magnetic mode to blue shift and weakens the radiation enhancement, which are same as the influences on the electric modes. The nonlocal response of electric and magnetic modes on various parameters of gap (width and refractive index) are investigated. The nonlocal effect strengthens as the gap narrows and the refractive index increases.

In the LAM simulation, a virtual dielectric layer is applied on the surface of metal whose permittivity ε_t and thickness Δd satisfies[21]

$$\frac{\varepsilon_t}{\Delta d} = \frac{\varepsilon_b \varepsilon_m q_L}{\varepsilon_m - \varepsilon_b}, \tag{1}$$

where ε_b and ε_m are the background permittivity and metal permittivity in the local model, and $q_L = \sqrt{\omega_p^2/\varepsilon_\infty - \omega(\omega + i\gamma)}/\beta$. $\beta = \sqrt{3/5}v_f$ is the nonlocal parameter derived from the hydrodynamic model[13,22], and v_f is the Fermi velocity. The metal permittivity in the LRA is determined by the Drude model:

$$\varepsilon(\omega) = \varepsilon_\infty - \frac{\omega_p^2}{\omega^2 + i\gamma\omega}. \tag{2}$$

We apply the LAM in a finite-domain time-domain simulation (Lumerical FDTD solutions) of the silver dimers. The minimum gap size is $d = 4$ nm, and the electron spill-out effect is neglected under such a circumstance[16,23,24]. The Drude parameters are taken as $\varepsilon_\infty = 4.007$, $\omega_p = 1.4 \times 10^{16}$, and $\gamma = 4.2176 \times 10^{13}$ according to the data from Ref. [25]. The value of $v_f = 1.39 \times 10^6$ m/s is taken for silver according to Ref. [15]. The thickness of the virtual layer is fixed at $\Delta d = 0.3$ nm.

When evaluating the ability to enhance the spontaneous emission of a nanoantenna, the Purcell factor is a vital parameter[26,27] that can be expressed as a decay rate enhancement relative to a vacuum. The ratio of the local density of states (LDOS) is also equal to it[28]:

$$F_p = \frac{\Gamma}{\Gamma_0} = \frac{\rho(\mathbf{r}_0, \omega)}{\rho_0(\mathbf{r}_0, \omega)}, \tag{3}$$

where, Γ_0 and $\rho_0(\mathbf{r}_0, \omega)$ are the decay rate and the LDOS in a vacuum. The power dissipated by the source can be calculated by the LDOS as $P_t = \frac{\pi\omega^2}{12\varepsilon_0}|\mu|^2\rho(\mathbf{r}_0, \omega)$. So the Purcell factor is calculated as the ratio of the dissipated powers with and without the nanoparticles:

$$F_p = \frac{P_t}{P_0}. \tag{4}$$

The radiation efficiency is expressed as the ratio of the radiated power and the total power dissipated as $\eta = P_r/P_t$. As a result, we can define the radiation enhancement as

$$F_r = \eta \times F_p = \frac{P_r}{P_0}. \tag{5}$$

The radiation enhancement gives us a balanced assessment of both the spontaneous enhancement and radiation efficiency.

In this Letter, we form a gap on the order of nanometers by combining two silver cuboids into a dimer. The structure is shown in Fig. 1(a). The size of the cuboids is 80 nm × 160 nm × 160 nm. A z-polarized electric dipole or y-polarized magnetic dipole is placed in the center of the gap, as shown in Figs. 1(b) and 1(c), to excite the electric or magnetic mode separately. In order to excite the electric and magnetic modes simultaneously, a z-polarized electric dipole is placed 20 nm away from the center along the x axis, as indicated by Fig. 1(d).

First of all, a local simulation is performed. The refractive index in the gap is 1.5, and the width is 10 nm. As shown in Fig. 2(a), when the electric dipole or magnetic dipole is placed at the center of the gap, either the electric mode at the wavelength of 695 nm or the magnetic mode at 725 nm is separately excited. If the z-polarized electric dipole is moved 20 nm along the x axis, two peaks at the wavelengths of 694 and 722 nm will be excited simultaneously. The spatial distribution of the electric field amplitude of the central xy plane in the gap is drawn to confirm that the displaced electric dipole properly excites the

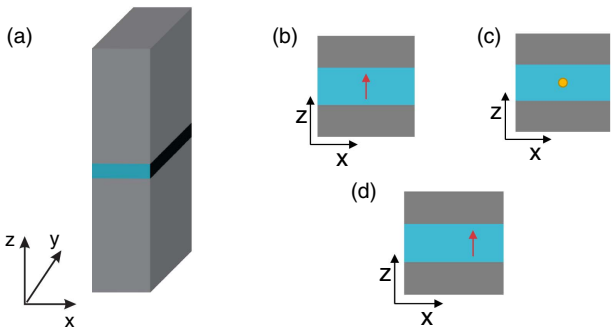

Fig. 1. (a) Silver dimer formed by a cuboid of 80 nm× 160 nm × 160 nm, (b)-(d) are schematics of three different excitations, (b) is the centered electric dipole, (c) is the centered magnetic dipole, and (d) is the 20 nm displaced electric dipole.

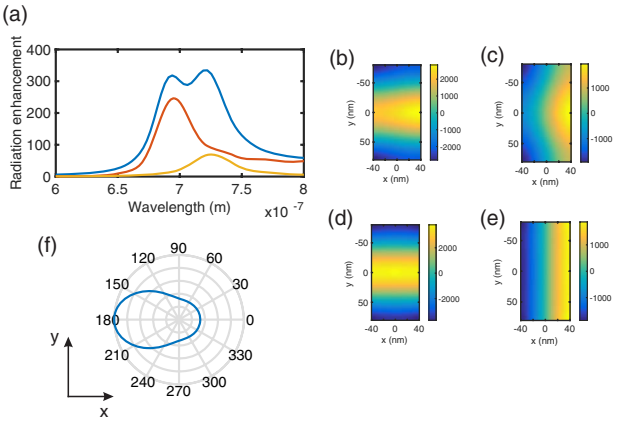

Fig. 2. (a) Spectra of the three excitations in the local model. blue line: the displaced electric excitation, red line: the center electric excitation, yellow line: the center magnetic excitation. (b) and (c) The spatial distributions of the electric field amplitude in the central xy plane of the gap of the displaced electric excitation at the peaks of 694 and 722 nm. (d) The spatial distribution of the electric field amplitude of the electric excitation at the peak of 695 nm. (e) The spatial distribution of the electric field amplitude of the magnetic excitation at the peak of 725 nm. (f) The normalized radiation pattern of the displaced electric excitation at 705 nm.

electric and magnetic modes. Figures 2(b) and 2(d) show that the electric field of the electric mode is spread along the y axis, and the magnetic mode has the electric field distributed along the x axis, as drawn in Figs. 2(c) and 2(e). The length and width of the silver cuboids along the x and y axes are tailored to be 80 and 160 nm to make the electric and magnetic modes close to each other, and unidirectional radiation similar to a Huygens' source[29,30] is achieved. The normalized radiation pattern is drawn in Fig. 2(f) at the 705 nm wavelength, which is at the center of the electric and magnetic peaks. The main lobe is along the negative x direction.

Then we analyze the same structure with the nonlocal model. Compared to the local model, the electric mode shifts from 695 to 681 nm and its radiation enhancement reduces from 246 to 229 in the nonlocal model, as shown in Fig. 3(a). The magnetic mode experiences similar changes of blueshift from 725 to 711 nm and radiation enhancement weakening from 69 to 65, as shown in Fig. 3(b). In Fig. 3(c), the blueshift and enhancement weakening caused by the nonlocal effect results in a stronger overlapping of the two modes when they are simultaneously excited. As a result, the two peaks no longer distinguish from each other. The radiation pattern of the displaced electric excitation at 695 nm still concentrates on the negative x direction, as shown by Fig. 3(d).

Next, the investigation of the gap width is performed. The refractive index in the gap is still 1.5. In the local model, the resonant wavelength of the electric mode shifts from 988 to 695 nm as the gap width increases from 4 to 10 nm, as shown by the blue dots in Fig. 4(a). In the nonlocal simulation, the resonant wavelength shifts from

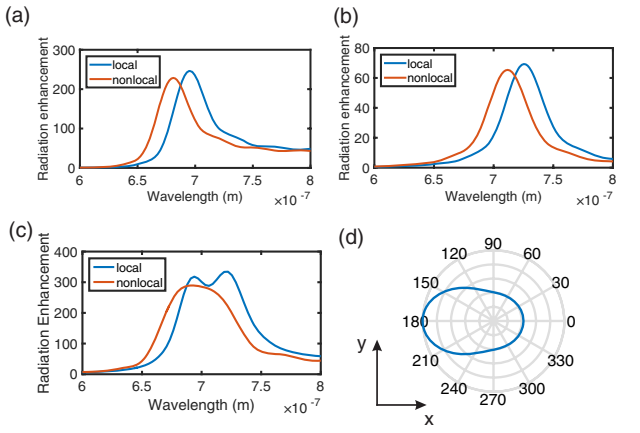

Fig. 3. (a) and (b) Spectrum comparisons of the local (blue line) and nonlocal (red line) model for solely electric and magnetic excitation. (c) The same comparison for the displaced electric excitation. (d) The normalized radiation pattern of the displaced electric excitation at 695 nm in the nonlocal model.

923 to 681 nm as the gap width increases, as shown by the red dots in Fig. 4(a). The nonlocal effect causes the resonant wavelengths to blue shift in all the situations of different gap widths. The maximum blueshift of 65 nm is reached in the 4 nm gap. For the magnetic mode, as shown in Fig. 4(c), the resonant wavelength shifts from 1014 to 725 nm when the gap width increases in the local model. Blueshift is caused by the nonlocal effect as well, which makes the resonant wavelength vary from 951 to 711 nm. As explained in the nonlocal hydrodynamic model, the metal charges spread a certain depth below the metal surface rather than distribute exactly on the surface[9,10]. This will make the gap width larger in the nonlocal model than in the local model in the view of surface charges. The blueshift of the resonant wavelength in the nonlocal model is the result of the "wider" gap. Figure 4(b) shows the nonlocal effect on the radiation enhancement of the electric mode. It decreases from 2666 to 246 when the gap varies

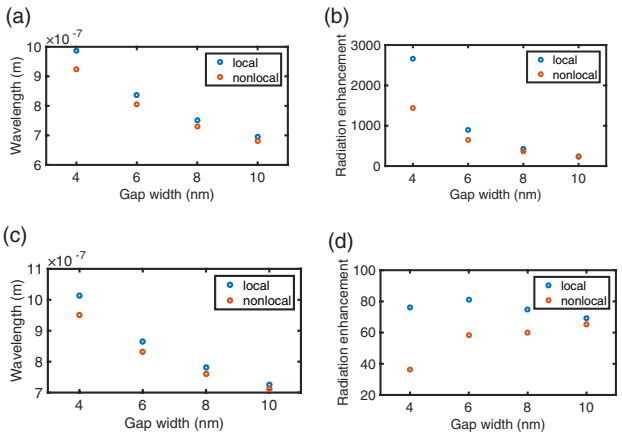

Fig. 4. (a) Wavelengths of the electric excited peaks in the local and nonlocal model and (b) is the corresponding radiation enhancement. (c) and (d) The same wavelength and enhancement results under magnetic excitation.

from 4 to 10 nm in the local model, but in the nonlocal model, this decrease is from 1444 to 228. The comparison of the radiation enhancement of magnetic mode in local and nonlocal mode is drawn in Fig. 4(d). The radiation enhancement stays at around 75, with different widths of gaps in the local model. In the nonlocal model, the weakening of the enhancement occurs again on the magnetic mode. As a result, the radiation enhancement is from 36 to 65 as the gap width increases in the nonlocal model.The nonlocal effect weakens the radiation enhancement and the weakening is stronger in the narrower gaps. In summary, when taking the nonlocal effect into consideration, the resonant wavelength is blue shifted and the radiation enhancement is weakened for both electric and magnetic modes. While the nonlocal effect is quite weak in the 10 nm gap, it cannot be neglected in smaller gaps.

Last, we give the relations between the nonlocal effect and the refractive index in the gap, which will be helpful for appropriately designing plasmonic systems for optimized fluorescence enhancement and efficient single-photon sources, etc. To display the strength of the nonlocal effect more directly, relative shifts of the wavelength and weakening of the radiation enhancement are calculated as $|\lambda^{\mathrm{local}}-\lambda^{\mathrm{nonlocal}}|/\lambda^{\mathrm{local}}$ and $|F_r^{\mathrm{local}}-F_r^{\mathrm{nonlocal}}|/F_r^{\mathrm{local}}$. The relative shifts of the resonant wavelength of electric and magnetic modes are shown in Figs. 5(a) and 5(c). The relative blueshift grows as the refractive index increases in the gap, and for a fixed refractive index the blueshift is larger in smaller gaps, as discussed above. The maximum blueshifts of electric and magnetic modes are reached in a gap of 4 nm width and a refractive index of 2 as 0.099 and 0.103, respectively. The relative enhancement weakenings are drawn in Figs. 5(b) and 5(d). When electrically excited, the enhancement weakening reaches a maximum of 0.475 in the 4 nm gap with a refractive index of 1.75. When magnetically excited, the maximum enhancement

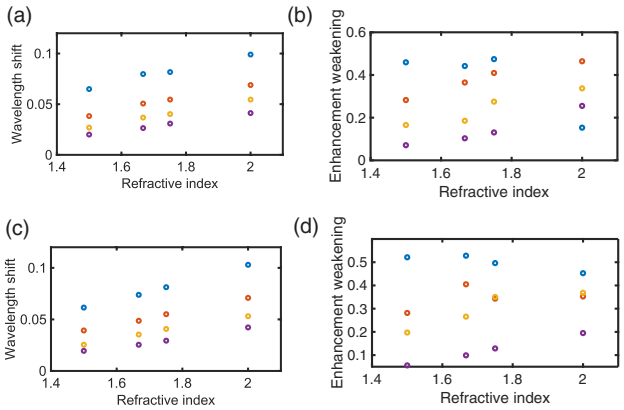

Fig. 5. Relative changes between the local and nonlocal model of different structures and excitations. (a) and (b) Wavelength shifts and enhancement weakenings under electric excitation, and (c) and (d) are wavelength shifts and enhancement weakenings under magnetic excitation. Blue dots are the results of a 4 nm gap, red ones are of a 6 nm gap, yellow ones are of a 8 nm gap, and purple ones are of a 10 nm gap.

weakening is 0.528 in the 4 nm gap, with a refractive index of 1.66.

In conclusion, we study the electric and magnetic resonances of a silver dimer in the nonlocal model. First, the nonlocal effect causes the electric and magnetic modes to blue shift. The unidirectional radiation that occurs in the overlapping region shifts as well, while the directivity remains. The relative shifts of the resonant wavelengths keep increasing when the gap width decreases and the refractive index increases. The largest relative shifts of 0.099 and 0.103 for electric and magnetic modes, respectively, are reached in the 4 nm gap with a refractive index of 2. Second, the radiation enhancement is weakened by the nonlocal effect. The maximum relative weakening of 0.475 of the electric mode is reached in the 4 nm gap, with a refractive index of 1.75 and for the magnetic mode it is 0.528 in the gap of 4 nm width and a refractive index of 1.66. We hope that this work will be helpful for appropriately designing plasmonic systems for optimized fluorescence enhancement and efficient single-photon sources.

This work was supported by the National Natural Science Foundation of China under Grant Nos. 11574293, 11274293, and 61377053.

References

1. M. Yi, D. Zhang, P. Wang, X. Jiao, S. Blair, X. Wen, Q. Fu, Y. Lu, and H. Ming, Plasmonics **6**, 515 (2011).
2. Z. Qi, J. Yao, L. Zhao, Y. Cui, and C. Lu, Photon. Res. **3**, 313 (2015).
3. C. Lü, J. Wang, X. Lü, and Z. Jia, Chin. Opt. Lett. **12**, S12401 (2014).
4. D. P. Fromm, A. Sundaramurthy, A. Kinkhabwala, P. J. Schuck, G. S. Kino, and W. E. Moerner, J. Chem. Phys. **124**, 061101 (2006).
5. W.-H. Tsai, K.-C. Lin, S.-M. Yang, Y.-C. Tsao, and P.-J. Ho, Chin. Opt. Lett. **12**, 042801 (2014).
6. R. F. Oulton, V. J. Sorger, T. Zentgraf, R. Ma, C. Gladden, L. Dai, G. Bartal, and X. Zhang, Nature **461**, 629 (2009).
7. J. Suh, C. Kim, W. Zhou, M. D. Huntington, D. T. Co, M. R. Wasielewski, and T. W. Odom, Nano. Lett. **12**, 5769 (2012).
8. L. Rogobete, F. Kaminski, M. Agio, and V. Sandoghdar, Opt. Lett. **32**, 1623 (2007).
9. G. Lu, J. Liu, T. Zhang, H. Shen, P. Perriat, M. Martini, O. Tillement, Y. Gu, Y. He, Y. Wang, and Q. Gong, Nanoscale **5**, 6545 (2013).
10. M. P. Busson, B. Rolly, B. Stout, N. Bonod, and S. Bidault, Nat. Commun. **3**, 962 (2012).
11. R. Alaee, C. Menzel, U. Hübner, E. Pshenay-Severin, S. Hasan, T. Pertsch, C. Rockstuhl, and F. Lederer, Nano Lett. **13**, 3482 (2013).
12. C. Ciracì, R. T. Hill, J. J. Mock, Y. Urzhumov, A. I. Fernandez-Dominguez, S. A. Maier, J. B. Pendry, A. Chilkoti, and D. R. Smith, Science **337**, 1072 (2012).
13. C. Ciracì, J. B. Pendry, and D. R. Smith, Chemphyschem. **14**, 1109 (2013).
14. N. A. Mortensen, Photon. Nanostruct. Fundam. Applic. **11**, 303 (2013).
15. S. Raza, M. Wubs, S. I. Bozhevolnyi, and N. A. Mortensen, Opt. Lett. **40**, 839 (2015).
16. R. Filter, C. Bösel, G. Toscano, F. Lederer, and C. Rockstuhl, Opt. Lett. **39**, 6118 (2014).
17. J. B. Lassiter, F. McGuire, J. J. Mock, C. Ciracì, R. T. Hill, B. J. Wiley, A. Chilkoti, and D. R. Smith, Nano Lett. **13**, 5866 (2013).
18. A. Rose, T. B. Hoang, F. McGuire, J. J. Mock, C. Ciracì, D. R. Smith, and M. H. Mikkelsen, Nano Lett. **14**, 4797 (2014).
19. G. M. Akselrod, T. Ming, C. Argyropoulos, T. B. Hoang, Y. Lin, X. Ling, D. R. Smith, J. Kong, and M. H. Mikkelsen, Nano Lett. **15**, 3578 (2015).
20. P. T. Bowen and D. R. Smith, Phys. Rev. B **90**, 195402 (2014).
21. Y. Luo, A. I. Fernandez-Dominguez, A. Wiener, S. A. Maier, and J. B. Pendry, Phys. Rev. Lett. **111**, 093901 (2013).
22. P. Halevi, Phys. Rev. B **51**, 7497 (1995).
23. T. V. Teperik, P. Nordlander, J. Aizpurua, and A. G. Borisov, Phys. Rev. Lett. **110**, 263901 (2013).
24. G. Toscano, C. Rockstuhl, F. Evers, H. Xu, N. A. Mortensen, and M. Wubs, Nat. Commun. **6**, 7132 (2015).
25. P. B. Johnson and R. W. Christry, Phys. Rev. B **6**, 4370 (1972).
26. A. F. Koenderink, Opt. Lett. **35**, 4208 (2010).
27. M. Agio and D. M. Cano, Nat. Photonics **7**, 674 (2013).
28. M. Agio, Nanoscale **4**, 692 (2012).
29. S. Campione, L. I. Basilio, L. K. Warne, and M. B. Sinclair, Opt. Express **23**, 2293 (2015).
30. Y. Wang, X. Zeng, E. Yang, Y. Lu, D. Zhang, and P. Wang, Chin. Opt. Lett. **14**, 011601 (2016).